This article has been accepted for publication in a future issue of this journal, but has not been fully edited. Content may change prior to final publication. Citation information: DOI 10.1109/TBME.2020.3036283, IEEE Transactions on Biomedical Engineering

Distortion of the Intracranial Pressure Waveform by Extraventricular Drainage System

Daniel Teichmann, *Member, IEEE*, James C. Lynch, *Student Member, IEEE*, Thomas Heldt, *Senior Member, IEEE*

***Abstract*— *Objective:* To investigate whether intracranial pressure (ICP) waveform measurements obtained from extraventricular drainage (EVD) systems are suitable for the calculation of intracranial elastance (ICE) or cerebrovascular pressure autoregulation (PAR) indices. *Methods:* The transfer characteristic of an EVD system is investigated by its step and frequency responses with particular focus on the low frequency (LF) range from 0.02 to 0.065 Hz (important for PAR estimation) and the location of the system's first resonance frequency (important for ICE estimation). The effects of opening the distal end of the EVD for drainage of cerebrospinal fluid and the presence of trapped air bubbles are also investigated. *Results:* The EVD system exhibits a first resonant frequency below 4 Hz, resulting in significant distortion of the measured ICP waveform. The frequency response in the LF range only remains flat when the EVD is closed. Opening the drain results in drops in magnitude and phase along the entire frequency range above DC. Air bubbles close to the EVD catheter tip affect the LF range while an air bubble close to the pressure transducer further decreases the first resonant frequency. Tests with actual ICP waveforms confirmed EVD-induced waveform distortions that can lead to erroneous ICE estimation. *Conclusion:* EVD-based ICP measurements distort the waveform morphology. PAR indices based on LF information are only valid if the EVD is closed. EVD-based ICE estimation is to be avoided. *Significance:* ICP waveform analyses to derive information about ICE and PAR should be critically questioned if only EVD derived ICP signals are at hand.**

***Index Terms*— Intracranial pressure, pressure measurement, extraventricular drainage, frequency response, step response**

This work was supported in part by the Deutsche Forschungsgemeinschaft (DFG, German Research Foundation) grant TE 1174/2-1, a grant from Philips Healthcare, and by a Cronin Graduate Fellowship in the Department of Electrical Engineering & Computer Science, Massachusetts Institute of Technology.

D. Teichmann, J.C. Lynch and T. Heldt are with the Institute for Medical Engineering and Science, Massachusetts Institute of Technology, Cambridge, MA 02139, USA (e-mail: teichi@mit.edu, jclynch@mit.edu, thomas@mit.edu).

D. Teichmann is also with SDU Health Informatics and Technology, The Maersk Mc-Kinney Moller Institute, University of Southern Denmark, 5230 Odense, Denmark.

J.C. Lynch and T. Heldt are also with the Research Laboratory of Electronics and the Department of Electrical Engineering and Computer Science, Massachusetts Institute of Technology, Cambridge, MA 02139, USA.

Copyright (c) 2020 IEEE. Personal use of this material is permitted. However, permission to use this material for any other purposes must be obtained from the IEEE by sending an email to pubs-permissions@ieee.org.

I. Introduction

INTRACRANIAL pressure (ICP) monitoring is common practice in the acute phase of severe head trauma, hemorrhagic stroke, and hydrocephalus, to alert care providers to elevated levels of ICP and the associated risk of secondary brain injury and the possibility of brain herniation [1]. While care guidelines base treatment recommendations on the mean level of ICP [2], [3], the ICP waveform exhibits characteristic intra-beat pulsations (Fig. 1), varies with the respiratory cycle, and also shows low-wave oscillations in the 0.3 to 3 cycles/min range [4], [5]. Analysis of these different waveform components has been explored for diagnostic and prognostic purposes [6].

Within a cardiac beat, up to five peaks, termed P_1 to P_5, have been reported [7], and a significant body of work has focused on mining such intra-beat morphological features for improved clinical decision making [8], [9], [10]. Such research has addressed the question of whether analysis of the ICP waveform morphology can aid in assessing the elastance of the intracranial space. A high intracranial elastance (ICE) indicates a potentially dangerous state in which a small increase in one of the intracranial compartment volumes causes a dramatic increase in ICP [1]. Cardoso *et al.* suggested that the ratio between the P_2 and P_1 amplitude (the P_2-to-P_1 ratio) is a quantifying measure of the ICE, with a ratio greater than unity indicating a compromised ICE [9]. Szewczykowski *et al.* analyzed the ICP (peak-to-peak) pulse amplitude as a function of mean ICP to assess ICE [8], and Czosnyka *et al.* introduced the RAP index as the correlation coefficient between the ICP pulse amplitude and the mean ICP [10].

Another line of investigation has focused on whether cerebral blood flow (CBF) autoregulation can be assessed through analysis of the slow-wave components of the ICP signal. In patients with severe traumatic brain injury, the cerebral vasculature's ability to regulate its own blood supply is thought to be impaired or entirely lost, thus putting the patients at significant risk of further injury if a mismatch occurs between the brain's metabolic substrate requirements and the systemic supply [11]. To this end, the Pressure Reactivity Index (PRx) is a dynamic indicator of pressure autoregulation that has attracted significant attention in the last two decades [12], [13], [14]. The PRx is based on the cerebrovascular vasomotor response to slow variations of ABP, that can be observed in the ICP signal's low frequency (LF) range between 0.02 to

This work is licensed under a Creative Commons Attribution-NonCommercial-NoDerivatives 4.0 License. For more information, see https://creativecommons.org/licenses/by-nc-nd/4.0/

This article has been accepted for publication in a future issue of this journal, but has not been fully edited. Content may change prior to final publication. Citation information: DOI 10.1109/TBME.2020.3036283, IEEE Transactions on Biomedical Engineering

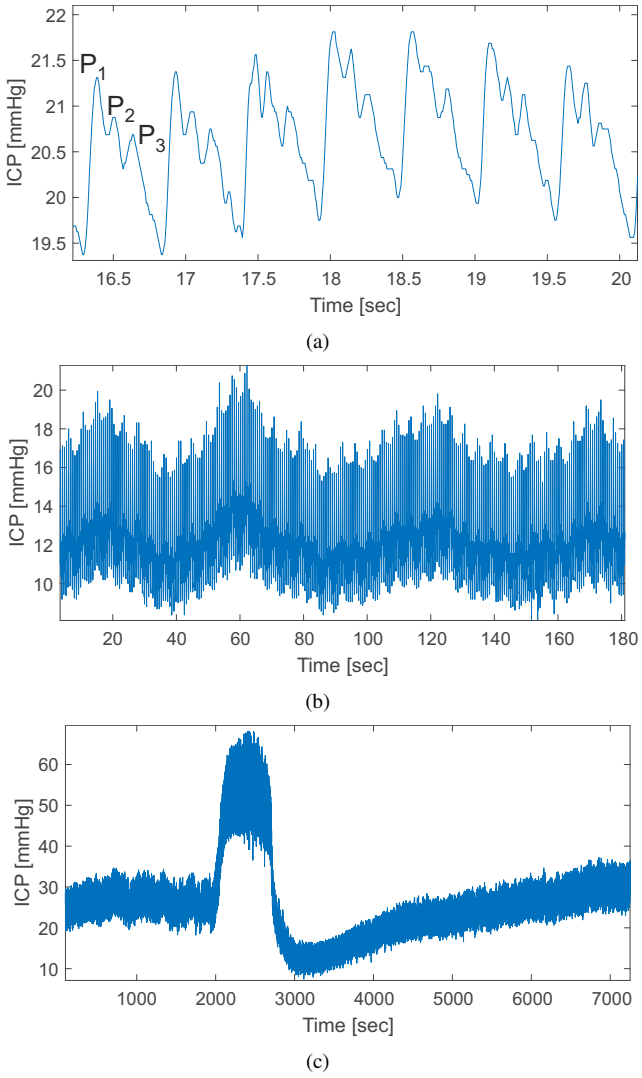

Fig. 1. ICP waveform. (a) Pulse waves with peaks P_1 to P_3. (b) Respiration and slow oscillations (B waves). (c) Plateau wave. Data in panel (c) courtesy of Prof. Marek Czosnyka, Addenbrooke's Hospital, Cambridge, UK.

0.065 Hz [15], and is calculated as the correlation coefficient between low-frequency variations in arterial blood pressure and ICP.

Whether analyzing the intra-beat or slow-wave oscillations in the ICP waveform, any inference depends on faithful and consistent measurement of the underlying ICP waveform across its various timescales. Clinically, ICP monitoring relies primarily on two methods, a parenchymal probe or an external ventricular drain (EVD). The parenchymal probe consists of a fiber-optic or micro-strain-gauge broad-bandwidth sensor at the tip of a thin catheter placed into the brain tissue. The EVD is a fluid-filled silastic catheter that is placed most often into one of the lateral ventricles for direct measurement of the cerebrospinal fluid (CSF) pressure. Additionally, the distal end of the EVD is commonly connected via long, elastic tubing to a drainage system that comprises a conventional clinical pressure transducer (pTD) and a height-adjustable outlet allowing for CSF removal. Thus, while the parenchymal probe transduces the pressure measured at the tip of the catheter, the EVD-based pressure measurement occurs at the distal end of elastic tubing that may itself act as a filter. While the frequency response (FR) of arterial catheter systems has been studied extensively to understand their transfer function characteristics for detailed waveform analysis of the arterial blood pressure (ABP) wavelet [16], the degree to which the fluid-filled EVD and associated drainage system distort the ICP waveform has not been investigated systematically.

In contrast to prior studies that have observed and evaluated exemplary clinically acquired data [17], [18], our work aims to determine the full FR characteristics between the input pressure at the tip of the EVD and the output pressure provided by the pTD at the distal end of the fluid-filled tubing of the drainage system. Additionally, we take a system-theoretic approach to model the transfer function and in a simulation step demonstrate how inference based on the EVD-based pressure measurements can be misleading about the state of brain health.

II. Materials and Methods

A. EVD-based ICP Monitoring

In clinical practice, an EVD catheter is placed with its tip into a lateral ventricle and connected with its distal end to an external drainage system (EDS), see Fig. 2. (Throughout this work, the combination of EVD catheter and EDS will be referred to as the EVD system.) The EDS provides a standardized tubing line that conducts the CSF to a three-way stopcock that can be opened towards a fluid-filled pTD to measure the CSF pressure and/or towards a small length of vertically-oriented tubing (downstream of the pTD) that forms an adjustable hydrostatic column with an outlet whose height can be adjusted. When the connection to this tubing is open, the vertical extent of column permits passive CSF drainage depending on the location of the outlet, thereby allowing clinicians to establish a desired ICP threshold above which CSF is being drained. While the connection to the pTD is typically always open so that ICP may be continuously monitored, the connection to the vertical drainage tubing is only open if elevated ICP is expected and CSF removal is desired (open drain). It is otherwise closed (closed drain). When the drain is open, two different techniques are commonly used in clinical practice: "Monitor First" (or "Intermittent Drainage") and "Drainage First" (or "Continuous Drainage") [19]. In Drainage First mode, CSF is continuously draining and only stops when the EVD is closed from time to time to record the true ICP level. Continuous drainage is achieved by placing the drip outlet at a height (typically between 7 cm to 15 cm) that is below the current ICP level but still high enough to avoid the collapse of the ventricle. In Monitor First mode, there is no drainage of CSF and the ICP is constantly monitored until a certain ICP threshold is reached, at which point CSF drainage begins in order to avoid higher ICP levels than the threshold. The threshold-triggered CSF drainage is usually achieved by placing the outlet at a height that corresponds to the ICP threshold level: a CSF column will rise within the short vertical tubing that connects the drip chamber with the stopcock and will start to drain into the drip chamber as soon as the ICP threshold is exceeded.

This work is licensed under a Creative Commons Attribution-NonCommercial-NoDerivatives 4.0 License. For more information, see https://creativecommons.org/licenses/by-nc-nd/4.0/

This article has been accepted for publication in a future issue of this journal, but has not been fully edited. Content may change prior to final publication. Citation information: DOI 10.1109/TBME.2020.3036283, IEEE Transactions on Biomedical Engineering

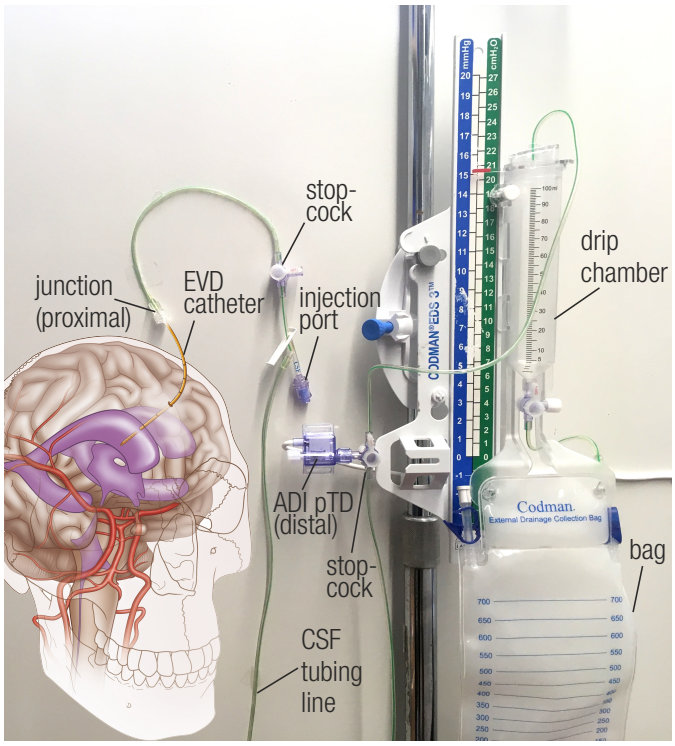

Fig. 2. Clinical set-up of the extraventricular drainage system. Anatomical drawing copyright Sara Jarret, CMI, Atlas InMedia. Published with permission.

While CSF drainage is taking place, the pressure reading of a pTD connected to the ventricle by fluid-filled tubing is thought to be unreliable. This may be due to two scenarios: 1) ventricle collapse when the drainage rate exceeds CSF production rate impeding further pressure propagation and 2) a pressure drop between the CSF pressure in the ventricle and in the EDS' pTD caused by the resistance of the catheter tip and the tubing [20], [21]. This is why the EVD is closed in Drainage First mode whenever a recording of the true mean ICP level is needed. However, in Monitor First mode, as long as there is no CSF flow, no collapse of the ventricle, and no air bubble in the system, the pressure reading of the EVD system is assumed to reflect the true mean ICP [20].

B. Experimental Setup

In this work, the transfer characteristics between the pressure at the EVD's tip and the pressure signal obtained by the pTD of the EDS are investigated, hence, the entire EVD system can be considered as the system under test (SUT).

We used a Codman EDS 3 Clear Ventricular CSF Catheter (Integra Lifesciences, USA) with a length of 35 cm and the Codman EDS 3 (Integra Lifesciences, USA) as test devices. Both are frequently used in clinical settings. The standardized tubing line of the Codman EDS 3 that connects the EVD catheter with the distal pTD is made of flexible silicone and is 168 cm long.

A pressure pulse generator (PPG; Model 601A, Flometrics Inc., USA) was used to generate pressure waveforms at the input of the SUT. The PPG uses a voltage-controlled piston mounted in an acrylic chamber with three Luer lock ports. The system is rated to generate pressures between 0 mmHg and 200 mmHg. We controlled the PPG with a waveform generator (33622A, Keysight Technologies, USA) using sinusoidal and square test waveforms of varying frequencies and amplitudes.

Deionized water was used to fill the acrylic chamber and the EVD and EVS tubing instead of CSF. The assumption of water as a good substitute for normal CSF was based on the grounds of normal CSF acting like a Newtonian fluid with shear viscosity similar to that of water over a wide range of shear stresses [22]. This may be a poor assumption in active bleeding and hemorrhagic strokes when the CSF protein and cell counts are increased, which will require further investigation. However, we assume that using a fluid comparable to clear CSF resembles the best case scenario for EVD-based ICP monitoring, as any addition of blood to the CSF would yield to even more distortion. Great care was taken to avoid introducing any air bubbles into the system. Unless stated differently, the system was operated in the closed-drain mode with the EVD catheter and CSF tubing line lying straight on and fixed to a table, and the output pTD connected to the distal connection point of the EDS (as depicted in Fig. 3). In no experiment was fluid draining out of the system, and therefore the net flow rate through the EDS was always zero. The DC baseline pressure level was achieved by setting a DC offset voltage on the PPG.

In all tests, the EVD catheter was inserted into the center port of the PPG chamber, and the connection was sealed with polytetrafluoroethylene tape. Additionally, we inserted a high-fidelity Millar catheter (SPR-524, Millar Inc., USA) into the chamber to precisely measure the reference pressure at the EVD tip. The Millar catheter has a solid-state pressure transducer at its tip that has a natural frequency of $\geq$10 kHz and therefore serves as the reference measurement P_{in} of the input pressure signal.

To measure what would be recorded by the system in a clinical setting, we connected a disposable pTD (MLT0699, ADInstruments, New Zealand) to the EDS's measurement port. Its signal will be referred to as the output pressure signal P_{out}. Both the input and output pTDs were connected to a data acquisition (DAQ) system (PowerLab 8/35, ADInstruments, New Zealand) via a quad bridge amplifier. The calibrated pressure signals as well as the waveform generator's output were simultaneously recorded with ADInstruments' LabChart software running on a computer connected to the DAQ. All signals were recorded with a sampling rate $f_s = 40$ kHz.

To assess the sensitivity of the transfer function characteristics to the particular choice of experimental conditions, we varied some of the experimental parameters as follows: 1) air bubbles of 0.5 or 1.0 ml were introduced into the system either close to the EVD's tip or within the output pTD slightly upstream of its membrane; 2) the drain was opened and the system was used in Monitor First mode; and 3) the DC level of the input pressure was raised from its baseline of 10 mmHg to 25 mmHg.

C. Assessment of the System's Transfer Characteristics

The transfer characteristics of the system were evaluated by determining the FR as well as the system's step response (SR).

This work is licensed under a Creative Commons Attribution-NonCommercial-NoDerivatives 4.0 License. For more information, see https://creativecommons.org/licenses/by-nc-nd/4.0/

This article has been accepted for publication in a future issue of this journal, but has not been fully edited. Content may change prior to final publication. Citation information: DOI 10.1109/TBME.2020.3036283, IEEE Transactions on Biomedical Engineering

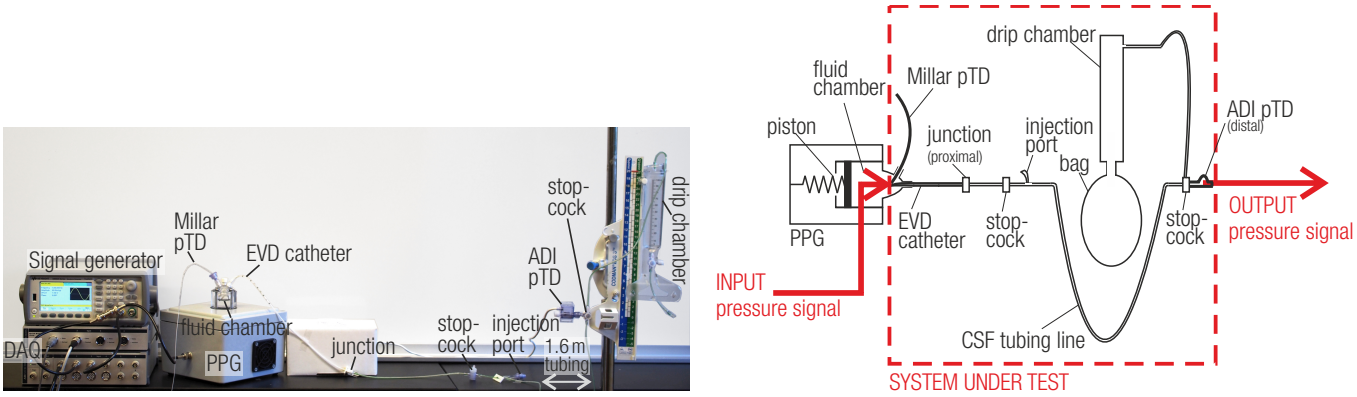

Fig. 3. a) Experimental set-up; and b) its schematic representation.

1) Frequency Response: The FR was derived by driving the PPG with a sinusoidal input signal whose frequency was varied from 0 to 50 Hz in increments of 0.1 Hz. Unless stated otherwise, the DC and peak-to-peak voltages of the input signal were chosen to achieve a DC pressure and peak-to-peak pressure amplitude in the acrylic chamber of 10 mmHg and 5 mmHg, respectively. The input signal was set to each frequency for 1 sec or at least 8 periodic cycles, whichever was longer. In some cases, additional recordings in the range of 0.01 to 0.7 Hz with increments of 0.005 Hz were conducted in order to allow a closer examination of the FR within the LF range. During these recording, the input signal was set to each frequency for at least 3 periodic cycles. By only observing the AC component rather than the DC of the signal, we suppress transient changes slower than the frequency under test.

For each frequency, the amplitude and phase of the input as well as output signal are determined by root mean square fitting of a sine with constant frequency but parameterized amplitude and phase to the signal recorded with the transducer. The magnitude of the FR was calculated by dividing the peak-to-peak amplitude recorded at the output pTD by the one recorded by the Miller catheter. The phase of the FR equals the phase lag of the output signal in relation to the input signal.

The Bode plots presented in Section III always show the FR of three repeated recordings in order to provide a sense of variability of the results. However, in some plots the lines are too close to be discernible in the chosen limits of the magnitude or phase axes.

2) Step Response: The system's SR was determined with an amplitude of 5 mmHg and an offset of 10 mmHg (i.e. release from 15 mmHg to 10 mmHg). Each measurement of a SR was repeated seven times, and the resultant SRs presented in Section III show the mean SR and the 95% confidence intervals.

The SRs were summarized by calculation of the damping coefficient D and the natural frequency f_n. The value (m_1 and m_2) and point in time (t_{m_1} and t_{m_2}) of the maxima of the first two oscillations after the falling edge as well as the baseline value during (b_1) and after (b_2) the step were captured (see Fig. 4). D and f_n were calculated according to [23] as

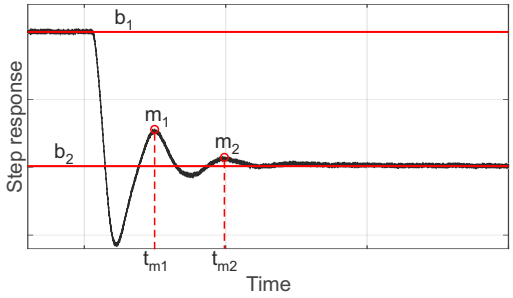

Fig. 4. A step response with the parameters used for calculation of the damping coefficient $\boldsymbol{D}$ and the natural frequency $\boldsymbol{f_n}$.

$$A = log(\frac{b_1 - b_2}{m_1 - m_2}) \tag{1}$$

$$D = \frac{A}{\sqrt{4\pi^2 + A^2}} \tag{2}$$

$$f_n = \sqrt{\frac{4\pi^2 + A^2}{2\pi(t_{m_1} - t_{m_2})}} \tag{3}$$

D. Feeding Real ICP Waveforms

To demonstrate and quantify the effect of the EVD system transfer characteristics on the ICP pulse wave morphology, we used exemplary measured ICP waveforms as input data for the EVD setup. These ICP waveforms were extracted from Cardoso et al. [9] who proposed the linkage between the P_2-to-P_1 ratio and ICE. Two different ICP waveform morphologies were extracted, one with low P_2-to-P_1 ratio, presumed to represent a state of low ICE, and the other with high P_2-to-P_1 ratio, presumed to represent a state of high ICE. Both waveforms were repeatedly concatenated with itself to resemble a continuous signal. These signals were fed into the waveform generator to drive the PPG while the variation of the ICP signal from the input pTD to the output pTD was observed. In order to be comparable with each other, the amplitude of both signals was adjusted so that the peak-to-peak pressure at the EVD's tip was 5 mmHg with a DC offset of 10 mmHg. Furthermore, the heart rate of the ICP signal,

This work is licensed under a Creative Commons Attribution-NonCommercial-NoDerivatives 4.0 License. For more information, see https://creativecommons.org/licenses/by-nc-nd/4.0/

This article has been accepted for publication in a future issue of this journal, but has not been fully edited. Content may change prior to final publication. Citation information: DOI 10.1109/TBME.2020.3036283, IEEE Transactions on Biomedical Engineering

and therewith the first fundamental frequency, was varied by compressing or stretching the input signal in time.

E. Modeling and System Identification

1) Transfer model: It has been demonstrated that phase delay, attenuation, and acoustic impedance are present in fluid-filled pressure tubing [24]. One approach to account for and succinctly summarize these observations is the form of a transmission line model. In each infinitesimal segment of the tubing, a series resistance per unit length R'_{tu} represents the viscous drag of the fluid on the catheter wall, a series inertance per unit length L'_{tu} represents inertia of the moving fluid, a parallel compliance per unit length C'_{tu} captures the stretch of the tubing wall, and a parallel leakage conductance per unit length G'_{tu} represents energy loss in the tube walls. The leakage conductance can be neglected since the viscoelastic property of the tubing material does not add significantly to the representation of the pressure tubing [25]. The pTD connected to the tubing exhibits additional resistance, inertance and compliance. Due to its small size, the compliance of the pTD's membrane is considered as a lumped element C_{tr}, while its resistance and inertance can be neglected [25].

The transmission line model with flexible tubing exhibits multiple resonant frequencies, which is in agreement with observation in experimental studies with fluid-filled arterial pressure tubing systems [26], [27]. However, if it is assumed that the lowest resonant frequency lies beyond the frequency range of interest, it has been shown that an one-section lumped model (only one lumped segment with a single R_{tu}, C_{tu}, L_{tu} component instead of infinitesimal segments) can sufficiently estimate the transfer characteristic [25]. Figure 5

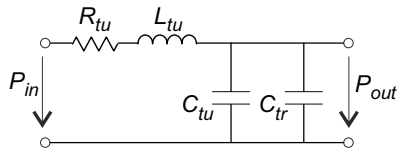

Fig. 5. Lumped model of the EVD system. $\boldsymbol{R_{tu}}$, $\boldsymbol{L_{tu}}$, and $\boldsymbol{C_{tu}}$ describe the resistance, inertance and capacitance of the tubing in its collective. $\boldsymbol{C_{tr}}$ is the compliance of the pTD's membrane.

shows such an one-section lumped model for the EVD-based ICP monitoring setup. The associated transfer function H of the system is:

$$H = \frac{P_{out}}{P_{in}} = \frac{1}{sC_{eq}(sL_{tu} + R_{tu}) + 1}, \tag{4}$$

with $C_{eq} = C_{tu} + C_{tr}$ and where R_{tu}, L_{tu}, and C_{tu} describe the aggregate resistance, inertance and capacitance of the tubing system.

ABP measurement systems have been found to behave like underdamped versions of such second-order systems [28], [29], [30] and can be described by D and f_n as given in Eqns 2 and 3. While a value of D between 0.6 and 0.7 is considered to be optimal [31], in clinical practice many systems happen to be immensely underdamped with D values between 0.13 and 0.35 [32], [31].

In comparison with common arterial lines, the setup of EVD-based ICP monitoring systems contain additional components. Instead of the combination of a stiff catheter and one tubing line with constant elastic properties along its length, the EVD system comprises a relatively long EVD catheter whose elastic properties are different from those of the EDS tubing line. Additionally, the EVD system comprises several intermediate sections with different properties (e.g., connection between EVD catheter and CSF line, injection port, proximal stopcock, and distal stopcock connecting to the pTD and the optional drainage line). Therefore, The EVD system might need to be represented by a higher-order model.

Effect of trapped air bubbles: Due to the high compressibility of air relative to water, any air bubble in the tubing will increase the total compliance of the system and thereby results in an undesirable decrease in the location of the resonant frequency. If air is assumed to be an ideal gas, then the gas volume is inversely related to the ambient pressure. Hence the compliance of the air bubble C_{bub} is related to the inverse of the square of the pressure [33]. This strong nonlinear function on pressure means that the additional compliance caused by the air bubble can be assumed to be constant only if the pressure variation is comparatively small. Furthermore, with higher static pressures, C_{bub} becomes smaller and hence f_r would become larger with increasing ICP values when air bubbles are present in the system [34].

Under no-flow conditions, the bubble can be modeled as a simple compliance shunting the transmission line [33]. This is illustrated by two second-order lumped transmission line circuits in series (Fig. 6), where l is the total length of the EVD catheter and EDS tubing line, x is the distance from the EVD catheter's tip and the location of the air bubble, and R'_{tu}, L'_{tu} and C'_{tu} are the tubing line's resistance, inertance and compliance per unit length (assuming that EVD catheter and EDS tubing line have the same physical properties). If

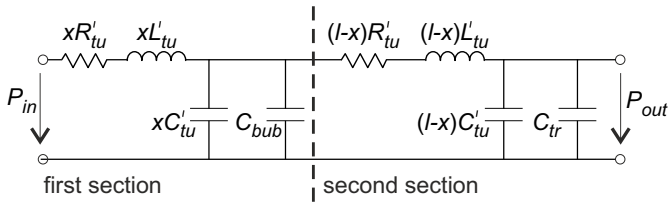

Fig. 6. Lumped model of the EVD system with a trapped air bubble. $\boldsymbol{C_{tr}}$ and $\boldsymbol{C_{bub}}$ are the compliance of the pTD membrane and air bubble, respectively. $\boldsymbol{R'_{tu}}$, $\boldsymbol{L'_{tu}}$ and $\boldsymbol{C'_{tu}}$ are the tubing line's resistance, inertance, and compliance per unit length. $\boldsymbol{x}$ is the distance between the source (EVD catheter's tip) and the air bubble. $\boldsymbol{l}$ is the total length of the tubing line.

we assume that C_{bub} is much larger than $C_{tu} = l \cdot C'_{tu}$ and C_{tr}, then the compliance of the first transmission line will be much larger than the compliance of the second, and the two second-order circuits are decoupled and resonate independently. The resonant frequencies of the first and second sections are approximately equal to $1/\sqrt{xL'_{tu}(xC'_{tu} + C_{bub})}$ and $1/\sqrt{(l-x)L'_{tu}[(l-x)C'_{tu} + C_{tr}]}$, respectively. The importance of this simplified model is the recognition that the location of the air bubble has an effect on the EVD system's performance in that the first resonant frequency decreases

This work is licensed under a Creative Commons Attribution-NonCommercial-NoDerivatives 4.0 License. For more information, see https://creativecommons.org/licenses/by-nc-nd/4.0/

This article has been accepted for publication in a future issue of this journal, but has not been fully edited. Content may change prior to final publication. Citation information: DOI 10.1109/TBME.2020.3036283, IEEE Transactions on Biomedical Engineering

with increasing distance between the air bubble and the EVD catheter's tip.

2) System identification: The transfer function of the EVD system was estimated using the `tfest` function of MATLAB's System Identification Toolbox (Release 2018a, MATLAB, The Mathworks, USA). Before the estimation run, the number of poles and zeros had to be chosen. Based on the model representation in Section II-E.1 and the recorded FR in Section III-A, the tested number of poles n_p, incremented by two, ranged from 2 to 8, while the number of zeros n_z was assumed to be 0.

The transfer function was estimated in two different ways. SR model: The transfer function that when applied to the step signal will produce the best fit to the recorded SR of the EVD system was estimated. FR model: The transfer function whose FR matches the recorded FR of the EVD system as exactly as possible was estimated.

The estimated transfer functions were validated with the elevated ICP signal that was described in Section II-D: The output of the estimated model based on this ICP input signal was calculated by multiplying the transfer function with the ICP signal (simulated output) and compared to the signal that was recored at the EVD system's output when fed with the ICP signal (true output). The comparison was performed by means of the normalized root mean squared error (NRMSE). The fit of a simulated output to a true output was calculated as $(1 - \text{NRSME}) \cdot 100)[\%]$.

III. Results

A. Transfer Characteristic

1) Closed drain: Figure 7 (a) presents the magnitude and phase of the FR of the entire closed EVD system. It can be observed that the EVD system comprises four resonant frequencies (local maxima in magnitude and corresponding drop in phase by π) at $\omega_1 = 3.7$ Hz, $\omega_2 = 9.1$ Hz, $\omega_3 = 26.9$ Hz, and $\omega_4 = 71.0$ Hz, respectively. The typical ICP pulse wave consists of its fundamental frequency which equals the heart rate and several higher harmonics. While some research on the ICP spectrum focus on the range from the fundamental to the fourth harmonic [35] other consider higher harmonics (up to the 9th harmonic) [36] for analysis. Assuming a possible heart rate range from 30 to 200 bpm, the frequency range of the first 4 harmonics would spread from 0.5 to 13.3 Hz. Even if we consider the best case scenario for the measurement system, i.e. the lowest heart rate of 30 bpm, the fourth harmonic would still lie at 2.70 Hz and the acquired ICP signal would be strongly distorted by the EDS. The first resonant frequency of the EVD system is therefore located well within the frequency range of the ICP waveform. There is a strong attenuation above 9 Hz and almost no attenuation or gain below 1 Hz. An increase in the DC offset of the sinusoidal input pressure waveforms to 25 mmHg had no effect on the FR (see Appendix).

In the LF range, it can be seen that the first resonant frequency already begins to affect the FR at 0.1 Hz as evidenced by the increase in gain and the lag in phase.

The result of the step-response is presented in Fig. 8 (a). The EVD system is underdamped $D = 0.20$, and the calculated natural frequency $f_n = 4.3$ Hz is in accordance with the first resonant frequency ω_1 obtained through the FR approach. (Note that the calculated f_n is slightly higher than ω_1 since the natural frequency corresponds to an undamped system).

2) Open Drain: As can be seen in Fig. 7 (b), an opening of the drain causes a strong attenuation over the entire frequency range above DC. Both magnitude and phase are reduced even at very low frequencies. The two higher resonant frequencies ω_3 and ω_4 are still visible, a local maximum at ω_2 can also still be observed, and around ω_1 the Bode plot exhibits a small notch in magnitude.

When comparing the SR of the entire system with closed (Fig. 8 (a)) and opened (Fig. 8 (b)) drain, we note three observations about the open drain system: i) The response overshoots and does not oscillate to values above the baseline; ii) it takes longer to settle to the baseline; iii) the signal-to-noise ratio is lower.

B. Air Bubbles

Fig. 7 (c) compares the FR of the EVD system without air bubble to that with trapped air bubbles. The introduction of a 0.5 ml air bubble close to and upstream of the pTD membrane results in the expected decrease of the first resonant frequency. This decrease becomes higher when the volume of the air bubble is increased from 0.5 ml to 1 ml. When the air bubble is located at the other end of the EVD system, close to and downstream of the EVD catheter's tip, other effects can be observed: i) The first resonant frequency is increased and ii) the magnitude shows an attenuation between 0 and 0.9 Hz (see also Fig.7 (d)).

C. Distortion of ICP Waves

Figure 9 shows the ICP pulse waveforms measured at the output pTD while the piston is driven with actual ICP waveform signals (black bold line) that are thought to be characteristic for low or high ICE levels (see Section II-D). Table I presents the corresponding P_2-to-P_1 ratios extracted from the recordings at the pTP. As can be seen in Fig. 9 the recorded ICP waveforms are significantly distorted by the fluid-filled EVD system. Consequently, the P_2-to-P_1 ratios as well as the peak to peak amplitude (AMP) given in Table I differ from those of the input waveforms.

As depicted in Fig. 10 the ICP pulse waveform comprises a fundamental frequency component and multiple higher harmonics. When this frequency spectrum is multiplied by the FR of the EVD system, this has the following influence on the ICP signal recorded by the pTD. For low heart rates, the fundamental frequency is lower than the resonance peak of the EVD system. As a result the amplitude of the fundamental frequency stays the same while the higher harmonics and therewith P_1 to P_5 are amplified. This yields a contradictory effect on different ICE indices.

For example, when comparing the P_2-to-P_1 ratio and AMP index calculated for the low ICE ground truth and its distorted ICP signal at a heart rate of 60 bpm, the AMP index is amplified by 42 % indicating an unhealthier brain state, while the P_2-to-P_1 ratio is slightly decreased by 8 % hinting towards

This work is licensed under a Creative Commons Attribution-NonCommercial-NoDerivatives 4.0 License. For more information, see https://creativecommons.org/licenses/by-nc-nd/4.0/

This article has been accepted for publication in a future issue of this journal, but has not been fully edited. Content may change prior to final publication. Citation information: DOI 10.1109/TBME.2020.3036283, IEEE Transactions on Biomedical Engineering

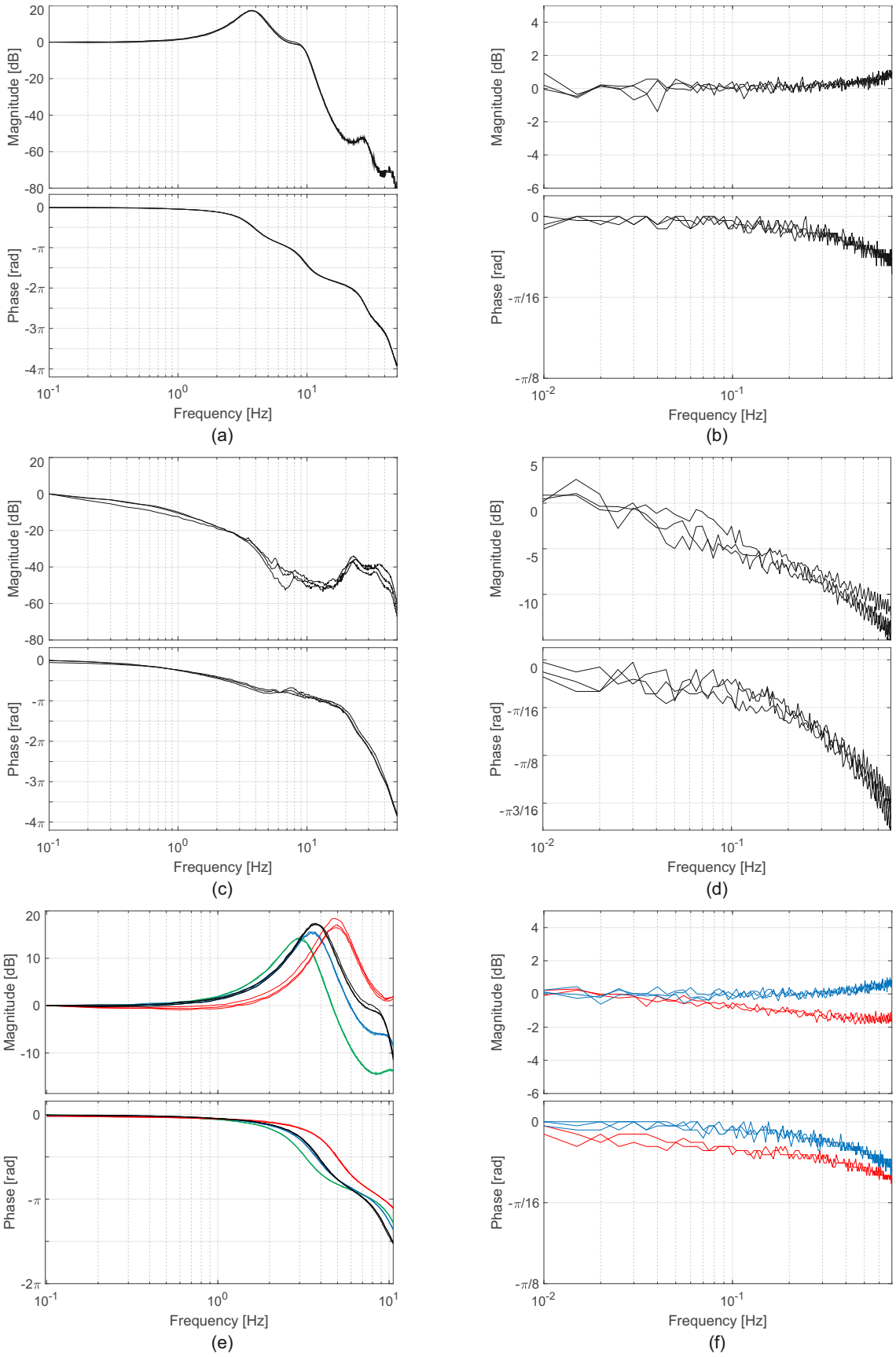

Fig. 7. Bode plot of the FR of the EVD system for the broad frequency range (left column) and the LF range (right column) measurement. (a+b): Closed drain. (c+d): Open drain, Monitor First mode. (e+f): Closed drain with no air bubble (black), 0.5 ml air bubble in front of pTD (blue), 1.0 ml air bubble in front of pTD (cyan), and 0.5 ml air bubble in EVD catheter (red).

This work is licensed under a Creative Commons Attribution-NonCommercial-NoDerivatives 4.0 License. For more information, see https://creativecommons.org/licenses/by-nc-nd/4.0/

This article has been accepted for publication in a future issue of this journal, but has not been fully edited. Content may change prior to final publication. Citation information: DOI 10.1109/TBME.2020.3036283, IEEE Transactions on Biomedical Engineering

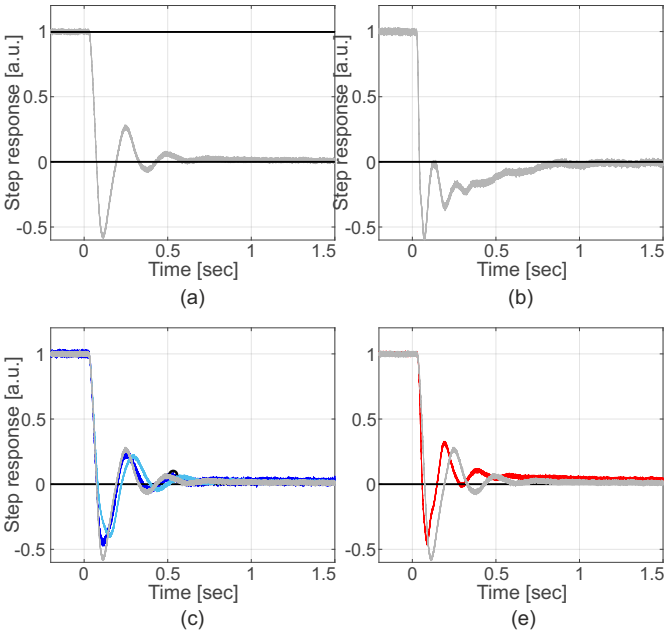

Fig. 8. SRs of the EVD system. (a): Closed drain, $\boldsymbol{D = 0.20}$, $\boldsymbol{f_n = 4.25}$ Hz. (b): Open drain, Monitor First mode. (c): Closed drain with no air bubble (grey), 0.5 ml air bubble in front of pTD (blue), $\boldsymbol{D = 0.21}$, $\boldsymbol{f_n = 3.62}$ Hz, 1.0 ml air bubble in front of pTD (green), $\boldsymbol{D = 0.24}$, $\boldsymbol{f_n = 3.69}$ Hz. (d): Closed drain with no air bubble (grey), 0.5 ml air bubble in the EVD catheter (red), $\boldsymbol{D = 0.18}$, $\boldsymbol{f_n = 5.3}$ Hz.

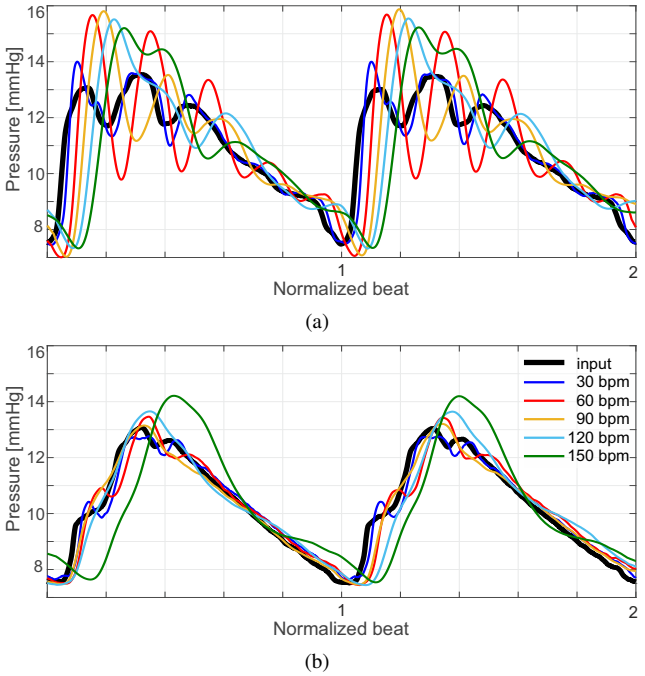

Fig. 9. ICP pulse waveforms measured at the output pTD while the input piston is driven with ICP data corresponding to (a) low and (b) high ICE levels according to [9]. The heart rate of the input waveforms was varied, but for better illustration and comparison of the waveform morphology, in this plot, the recorded ICP signals are stretched to the same width on the x axis.

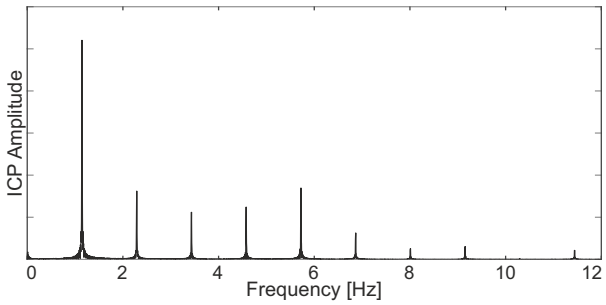

Fig. 10. Typical frequency spectrum of an ICP waveform.

a healthier brain state. A change in heart rate from 60 bpm to 90 bpm further decreases the P_2-to-P_1 ratio by 13 % although the ground-truth has not changed. For high heart rates, the fundamental frequency shifts into the region of the resonance peak and becomes the most amplified component of the pulse signal. This results in an increase in pulse amplitude (higher AMP index, unhealthier brain state) but also in a rounding of the pulse wave. Such rounding has previously been linked to an increasing ICE [37], [38]. In case of the elevated ICE level input signal, the P_1 peak is almost completely vanished at heart rates of 120 or 150 bpm.

The described distortions are more pronounced for the low ICE level example. This is because the low ICE level ground-truth signal presents more energy at the higher harmonics and those are (depending on the heart rate) mostly distorted by the EDS.

D. System Identification

Table II shows the results of the system identification based on the FR as well as SR. It shows the fit of the different models to the estimation data (estimation fit) as well as the fit of the simulated ICP output to the validation data set's ground-truth (validation fit) as described in Section II-E.2.

When using the SR as basis for the model estimation, the model with $n_p = 4$ resulting in two resonant frequencies performed best. The simulated ICP output yielded a 92.7 % fit. The models derived from the FR yielded better fits to its estimation data as well as validation data with higher system orders. However, overall they performed slightly worse than the models identified from the SR. Figure 11 presents the simulated output of the best SR ($n_p = 4$) and FR ($n_p = 8$) models when fed with the ICP input signal of the validation data set.

The Bode plot in Fig. 12 presents the FR of these models together with the true FR of the EVD system. The difference between the location of the first resonant frequency of the SR model and FR model is 0.06 Hz. The estimated values of the model parameters can be found in the Appendix V-B. While the SR model only models the transfer characteristic of the first two resonant frequencies (as it only has $n_p = 4$) and consequently misses 2π of phase drop, it matches the true magnitude around the first resonant frequency and below more accurately than the FR model. The later comprises the third and fourth resonant frequency, but the respective peaks in magnitude are too sharp and the location of the fourth resonant frequency is off.

To test the sensitivity of the model estimation and check for overparameterization, we added i.i.d. noise uniformally distributed within an interval of 5 % of the maximum amplitude

This work is licensed under a Creative Commons Attribution-NonCommercial-NoDerivatives 4.0 License. For more information, see https://creativecommons.org/licenses/by-nc-nd/4.0/

This article has been accepted for publication in a future issue of this journal, but has not been fully edited. Content may change prior to final publication. Citation information: DOI 10.1109/TBME.2020.3036283, IEEE Transactions on Biomedical Engineering

TABLE I

EXTRACTED P_2-TO-P_1 RATIO (P_2/P_1), PEAK-TO-PEAK AMPLITUDE (AMP), AND AMPLITUDE OF THE FUNDAMENTAL HARMONIC (FH AMP) EXTRACTED FROM ICP WAVEFORMS MEASURED AT THE OUTPUT PTD WHILE THE PISTON IS DRIVEN WITH ICP DATA OF LOW AND HIGH ICE LEVELS ACCORDING TO [9]. BRACKETS INDICATE VALUES WHICH WERE NOT CLEARLY EXTRACTABLE.

ICE level	heart rate	P_2/P_1	Amp [mmHg]	FH Amp [mmHg]
low	ground truth	1.04	6.03	2.00
	30 bpm	0.97	6.55	1.88
	60 bpm	0.96	8.61	2.03
	90 bpm	0.85	8.79	2.01
	120 bpm	0.84	8.20	2.32
	150 bpm	0.95	7.88	2.61
elevated	ground truth	1.32	5.55	2.30
	30 bpm	1.22	5.09	2.13
	60 bpm	1.24	5.97	2.11
	90 bpm	1.22	5.74	1.85
	120 bpm	(1.27)	6.33	2.39
	150 bpm	(1.39)	6.66	2.65

TABLE II

RESULT OF THE SYSTEM IDENTIFICATION. ESTIMATION WAS EITHER BASED ON THE SYSTEM'S SR (SR MODEL) OR FR (FR MODEL).

	SR model		FR model	
n_p	estimation fit	validation fit	estimation fit	validation fit
2	93.2 %	89.8 %	54.6 %	79.7 %
4	95.9 %	92.7 %	84.7 %	84.3 %
6	90.8 %	77.2 %	88.0 %	86.5 %
8			89.7 %	87.4 %

of the SR and FR, respectively, and identified a SR model with $n_p = 4$ and a FR model with $n_p = 8$ with this noisy data. The average deviation of the estimated parameter values compared with the ones estimated based on the noise free data was 0.17 % and 3.14 % for the SR and FR model. The estimation fit for both models dropped slightly (SR: 91.5 %, FR: 82.7 %) as noise was added while the validation fit stayed almost the same (SR: 92.7 %, FR: 87.7 %).

IV. DISCUSSION

The EVD system used for our recordings is an underdamped system of at least 8th order. The obtained damping coefficients in this study are low but lie in a value range that has been reported for ABP measurements elsewhere. We decided to not use any additional mechanical damping device ([39]) or parallel damping technique ([28]) as this does not seem to be common clinical practice and has also only been seldomly used in clinical studies investigating the ICP pulse wave morphology or pressure autoregulation responses. Furthermore, the recordings in this study indicate the first resonant frequency of the closed EVD system of $\omega_1 = 3.7$ Hz, which is much lower than the first resonant frequencies reported by studies about arterial line measurements. In order to ascertain the validity of our setup as well as of our algorithm to obtain the FR, we utilized the same methodology to determine the FR of a tubing line for invasive ABP measurement (length 20 cm with a closed three-way stopcock at its end). The resulting FR can be found in the Appendix (Fig. 15) and shows the first resonant frequency above 30 Hz, which is in agreement with reported values and would allow precise ABP waveform recordings.

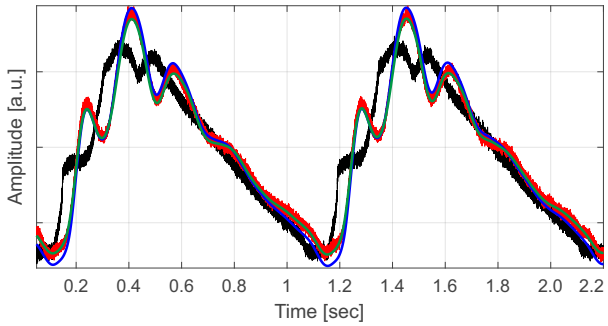

Fig. 11. Simulated output of the best SR and FR model when fed with an ICP input signal. Black: ICP input signal; red: recorded ICP output signal; green: simulated output signal of the SR model with $n_p = 4$; blue: simulated output signal of the FR model with $n_p = 8$.

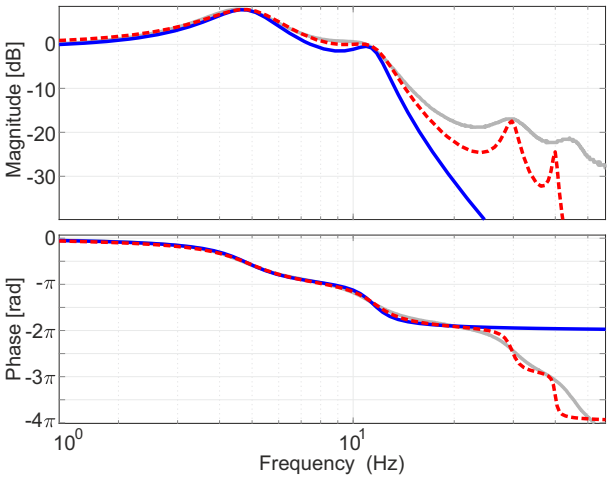

Fig. 12. Bode plot of the FRs of the SR model with $n_p = 4$ (blue), the FR model with $n_p = 8$ (red), and the true, recorded characteristic of the EVD system (grey).

Therefore, we conclude that our setup and analysis technique are valid and that the EVD system's first resonance frequency is indeed this low. The current study only considers normal CSF. Future studies are needed to investigate the degree to which CSF in hemorrhagic injuries alter the transfer function characteristics of the EVD system. Another point that has not been taken into consideration here, is the EVD's proneness to motion artifacts that can be easily induced by touching or readjusting the EVD system and can cause significant distortions in the measurement line.

The requirement for ABP systems in order to be considered accurate enough to analyze the waveform for systolic and diastolic pressures is that the system should not distort frequencies of 15 Hz to 20 Hz more than 5% [16] and hence the first resonant frequency has to be at least above 20 Hz. In the EVD system under evaluation, this requirement is not fulfilled, the first resonant frequency lies at 3.7 Hz so that for heart rates above 60 bpm even the fundamental frequency of the pulse wave will be distorted by the relatively broad resonant peak. Therefore, we conclude that diagnosis made on basis of the ICP pulse waveform should be avoided, if the signal has been recorded with a setup similar to ours. Such diagnosis includes the calculation of an ICE index. This also became apparent

This work is licensed under a Creative Commons Attribution-NonCommercial-NoDerivatives 4.0 License. For more information, see https://creativecommons.org/licenses/by-nc-nd/4.0/

This article has been accepted for publication in a future issue of this journal, but has not been fully edited. Content may change prior to final publication. Citation information: DOI 10.1109/TBME.2020.3036283, IEEE Transactions on Biomedical Engineering

when testing the EVD system with ICP pulse waveforms (see Fig. 9). The distortion of the ICP pulse waveform introduced by the EDS, will have a significant influence onto ICE indices and the estimation of the current brain health. This becomes especially complicated as not only the magnitude but also the direction of falsification, i.e. if the distortion falsifies towards false positives or false negatives, can vary. It depends on the actual ICP pulse waveform morphology, the heart rate, and the choice of ICE index. In this context, one might also critically review studies describing such ICE indices: The established ICE indices by Cardoso et al. (P_2-to-P_1 ratio), Szewczykowski et al. (AMP index), and Czosnyka et al. (RAP index) have been introduced based on ICP measurements acquired with fluid-filled silastic catheters and tubes [9], [8], [10]. Other studies investigating the ICE by analyzing the FR between the ABP and the ICP were also based on EVD catheters [40], [41]. There is another group of studies that utilized rigid needles instead of EVD catheters but still used elastic tubing to connect the needle to a fluid-filled pTD [42], [37]. In a further set of studies the precise description of the ICP measurement is lacking [6], [43]. In contrast to other ICE indices, the RAP does not depend on the absolute amplitude value of the ICP pulse wave (or the amplitude differences between specific points along the waveform) and may therefore be less (or not at all) affected by distortions introduced by the EVD system. One way to verify the robustness of the RAP under EVD-based ICP measurements would be to compute the undistorted ICP waveform from the EVD-based measured ICP waveform (see below) and determine whether the RAP index recovered from the reconstructed waveform leads to different conclusions than the one determined from the measured ICP waveform.

Within the LF range the FR's magnitude and phase stayed flat, so that the determination of cerebrovascular pressure autoregulation with the PRx index is plausible with EVD-based ICP monitoring during closed-drain mode. However, when the distal outlet is opened and the EVD system is utilized in Monitor First mode, a fluid column will establish in the short line connecting the stopcock and the drip chamber and will serve as a large compliance as its height varies with the input pressure. This results in a drop of magnitude and phase along the entire frequency range (Fig. 7 (c)). The pulse wave content will diminish and the LF range is corrupted in a way that may affect accurate PRx determination.

The introduction of a trapped air bubble close to the pTD dome resulted in a decrease of the first resonant frequency as it would be expected according to the simplified model described in Section II-E.1. What is more surprising, is the observation that the first resonance frequency increased when the air bubble was trapped at the other end of the EVD system within the EVD catheter near the catheter's tip. Due to the fact that the air bubble is located near the very beginning of the EVD system, its distance x to the source approaches zero and so will the resistance and inertance of the first second order section (see Fig. 6). Its compliance will still be larger than the one of the second circuit, because $C_{bub} \gg C_{tu}, C_{tr}$, but since the inertance is diminished, the first circuit does not oscillate but serves as a low pass (compare magnitude in Fig. 7 (f)). As a consequence, the resonant frequency of the second circuit will become the first resonant frequency of the entire system. This resonant frequency will be higher than the first resonant frequency of the air bubble free system, because $(l - x) < l$. Besides this attempt of explanation, the significance of this observation is that while an air bubble will always degrade the performance of the measurement system, an air bubble located close to the catheter tip will have more effect on the transfer characteristic in the LF range and an air bubble located closer to the pTD will have more effect on the distortion of the pulse wave morphology. However, to substantiate this claim a more detailed investigation would be needed to determine the effect of an air bubble when its location is systematically varied along the tubing line.

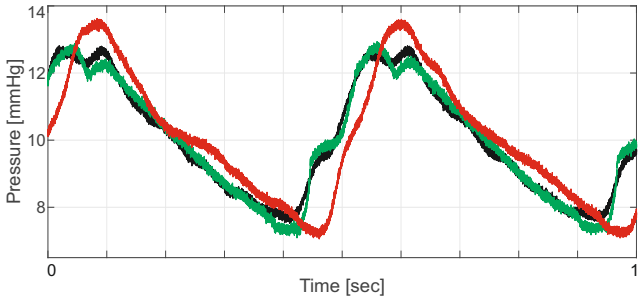

Fig. 13. Correction of ICP pulse waveforms by deconvolution in the frequency domain. Black: original ICP signal; red: distorted ICP signal; green: reconstructed ICP waveform.

The experiments of this study (see Section III-D) showed that in the case of an EVD system, a 4th order system allows to accurately predict the ICP recording with a fit of 92.7 %. The higher order models ($n_p > 4$) derived from the SR did not perform as well the ones for lower orders. This might be due to the signal noise of the output pTD and due to the limited frequency content of the input signal used for validation. Overall, the SR model yielded better estimation than the FR model. A possible explanation is that the location of the first resonant frequency of the SR model matches the one of the true FR of the closed EVD system more accurately, because the frequency resolution of the SR analysis ($f_s = 40$ kHz) is higher than the frequency resolution of the sinusoidal analysis (increments of 0.1 Hz).

Once the transfer function of the EVD system is identified, the distorted ICP recording may be corrected by inverse modeling techniques. Here, we realized the ICP waveform reconstruction by deconvolution in the frequency domain in which we multiplied the Fourier transformed distorted ICP signal $Y(j\omega)$ by the inverse of the EVD's transfer function $H(j\omega)^{-1}$ to obtain an estimate $\hat{X}(j\omega)$ of the Fourier transform $X(j\omega)$ of the original waveform. $\hat{X}(j\omega)$ can then be transformed back into the time domain by inverse Fourier transform. Figure 13 shows a deconvolution-based reconstruction of the input ICP waveform to the EVD. The frequency domain deconvolution has only been applied within the frequency range of 0 to 15 Hz, as otherwise high frequency components may be greatly amplified. In future explorations, Wiener Deconvolution may be considered to recover the undistorted ICP waveform [44].

This work is licensed under a Creative Commons Attribution-NonCommercial-NoDerivatives 4.0 License. For more information, see https://creativecommons.org/licenses/by-nc-nd/4.0/

This article has been accepted for publication in a future issue of this journal, but has not been fully edited. Content may change prior to final publication. Citation information: DOI 10.1109/TBME.2020.3036283, IEEE Transactions on Biomedical Engineering

V. Conclusion

The EVD system used in this study is at least an 8th order system and exhibits four resonant frequencies. Given an ICP input signal, the output generated by the EVD system can be simulated by a 4th order model estimated based on the SR with a fit of 92.7 %.

When using an EVD setup similar to one in this study, the first resonant frequency is very low and, hence, the ICP pulse waveform is distorted so that diagnosis made on basis of the ICP pulse waveform should be avoided and the estimation of ICE indices is not recommendable as it is unpredictably misleading, dependant on the heart rate and inconsistent among different ICE indices. The FR in the LF range is flat, implying that the estimation of the PRx pressure autoregulation index remains uncorrupted as long as the drain is closed. When the drain is open, the magnitude and phase exhibit a drop across the frequency range, even affecting the ICP signal within the LF range.

The presence of a trapped air bubble always degrades the system's performance, but depending on the location of the air bubble the LF or the pulse frequency range is more affected: An air bubble near the pTD has mainly a worsening effect on ICE index estimation while an air bubble located close to the EVD catheter's tip mainly degrades PRx estimation.

APPENDIX

A. Bode plots

Figures 14 and 15 show the Bode plots of the FR of the closed EVD system with a DC offset of 25 mmHg and of an EVD system with a short tubing line, respectively.

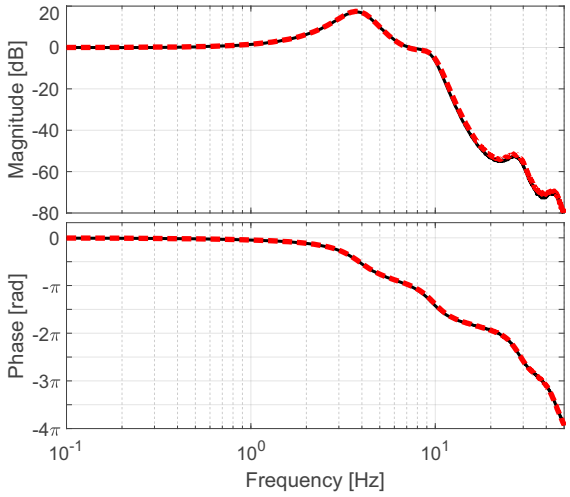

Fig. 14. Bode plot of the FR of the closed EVD system with (red, dashed line) an increased DC offset of the sinusoidal input waves of 25 mmHg. For comparison the FR of the same system but with a DC offset of the sinusoidal input waves of 10 mmHg (as in Fig. 7 (a)) is plotted in black.

B. Model parameters

Since the estimated models have no zero, the numerator of the estimated transfer function H is always one. The number of parameters b_i in the denominator equals the number of poles n_p.

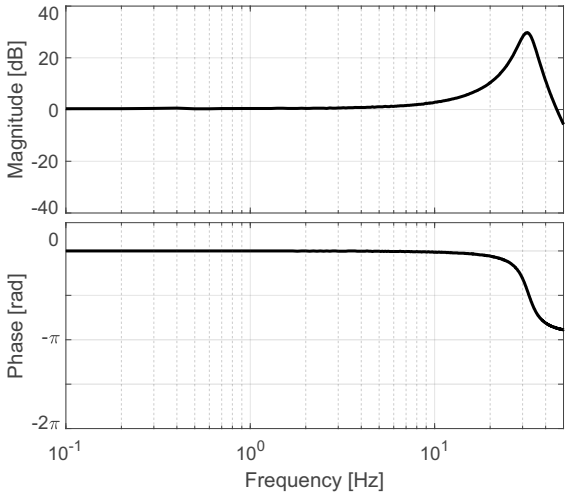

Fig. 15. Bode plot of the FR of a short tubing line for invasive ABP measurement.

$$H = \frac{1}{b_{n_p} s^{n_p} ... + b_2 s^2 + b_1 s^1 + b_0} \tag{5}$$

TABLE III
Estimated parameter values b_i of the SR model. n_p denotes the number of poles.

	$n_p = 2$	$n_p = 4$	$n_p = 6$
b_6			$2.9\,e^{-11}$
b_5			$5.2\,e^{-9}$
b_4		$2.3\,e^{-10}$	$5.9\,e^{-7}$
b_3		$6.7\,e^{-9}$	$3.3\,e^{-5}$
b_2	$1.2\,e^{-3}$	$1.4\,e^{-6}$	$2.0\,e^{-3}$
b_1	$1.4\,e^{-2}$	$2.0\,e^{-5}$	$3.6\,e^{-2}$
b_0	1.09	1.09	1.09

TABLE IV
Estimated parameter values b_i of the FR model. n_p denotes the number of poles.

	$n_p = 2$	$n_p = 4$	$n_p = 6$	$n_p = 8$
b_8				$8.7\,e^{-17}$
b_7				$5.4\,e^{-15}$
b_6			$6.2\,e^{-12}$	$9.2\,e^{-12}$
b_5			$3.0\,e^{-10}$	$4.6\,e^{-10}$
b_4		$1.9\,e^{-7}$	$2.4\,e^{-7}$	$2.5\,e^{-7}$
b_3		$6.7\,e^{-6}$	$8.5\,e^{-6}$	$9.9\,e^{-6}$
b_2	$1.0\,e^{-3}$	$1.2\,e^{-3}$	$1.4\,e^{-3}$	$1.3\,e^{-3}$
b_1	$1.3\,e^{-2}$	$1.9\,e^{-2}$	$2.1\,e^{-2}$	$2.1\,e^{-2}$
b_0	0.9	0.9	1.0	1.0

References

[1] T. Heldt *et al.*, "Intracranial pressure and intracranial elastance monitoring in neurocritical care," *Ann. Rev. Biomed. Eng.*, vol. 21, pp. 523–549, 2019.

[2] N. Carney *et al.*, "Guidelines for the management of severe traumatic brain injury," *Neurosurg.*, vol. 80, no. 1, pp. 6–15, 2017.

[3] P. M. Kochanek *et al.*, "Guidelines for the management of pediatric severe traumatic brain injury," *Ped. Crit. Care*, vol. 20, no. 3, pp. 280–289, 2019.

This work is licensed under a Creative Commons Attribution-NonCommercial-NoDerivatives 4.0 License. For more information, see https://creativecommons.org/licenses/by-nc-nd/4.0/

This article has been accepted for publication in a future issue of this journal, but has not been fully edited. Content may change prior to final publication. Citation information: DOI 10.1109/TBME.2020.3036283, IEEE Transactions on Biomedical Engineering

[4] N. Lundberg, "Continuous recording and control of ventricular fluid pressure in neurosurgical practice," *Acta Psych. Scand. Suppl.*, vol. 36, no. 149, pp. 1–193, 1960.

[5] Z. Czosnyka *et al.*, "CSF pulse pressure and B waves," *J. Neurosurg.*, vol. 103, no. 4, pp. 767–768, 2005.

[6] C. Robertson *et al.*, "Clinical experience with a continuous monitor of intracranial compliance," *J. Neurosurg.*, vol. 71, no. 5, pp. 673–680, 1989.

[7] A. Gega *et al.*, "Analysis of the wave pattern of CSF pulse wave," in *Intracranial Pressure IV*, K. Shulman *et al.*, Eds. Berlin, Heidelberg: Springer Berlin Heidelberg, 1980, pp. 188–190.

[8] J. Szewczykowski *et al.*, "A fast method of estimating the elastance of the intracranial system," *J. Neurosurg.*, vol. 47, no. 1, pp. 19–26, 1977.

[9] E. R. Cardoso *et al.*, "Analysis of the cerebrospinal fluid pulse wave in intracranial pressure," *J. Neurosurg.*, vol. 59, no. 5, pp. 817–821, 1983.

[10] M. Czosnyka *et al.*, "Analysis of intracranial pressure waveform during infusion test," *Acta Neurochir.*, vol. 93, no. 3-4, pp. 140–145, 1988.

[11] C. Lazaridis *et al.*, "Optimal cerebral perfusion pressure: are we ready for it?" *Neurol. Res.*, vol. 35, no. 2, pp. 138–148, 2013.

[12] M. Czosnyka *et al.*, "Continuous assessment of the cerebral vasomotor reactivity in head injury," *Neurosurg.*, vol. 41, no. 1, pp. 11–7; discussion 17–9, 1997.

[13] M. Czosnyka, "Monitoring and interpretation of intracranial pressure," *J. Neurol. Neurosurg. Psych.*, vol. 75, no. 6, pp. 813–821, 2004.

[14] M. Czosnyka *et al.*, "Pressure reactivity index: journey through the past 20 years," *Acta Neurochir.*, vol. 159, no. 11, pp. 2063–2065, 2017.

[15] T. Howells *et al.*, "An optimal frequency range for assessing the pressure reactivity index in patients with traumatic brain injury," *J. Clin. Monit. Comput.*, vol. 29, no. 1, pp. 97–105, 2015.

[16] H. A. Schwid, "Frequency response evaluation of radial artery catheter-manometer systems: sinusoidal frequency analysis versus flush method," *J. Clin. Monit.*, vol. 4, no. 3, pp. 181–185, 1988.

[17] M. J. H. Aries *et al.*, "Observation of autoregulation indices during ventricular csf drainage after aneurysmal subarachnoid hemorrhage: A pilot study," *Neurocrit. Care*, vol. 23, no. 3, pp. 347–354, 2015.

[18] T. Howells *et al.*, "The effects of ventricular drainage on the intracranial pressure signal and the pressure reactivity index," *J. Clin. Monit. Comput.*, vol. 31, no. 2, pp. 469–478, 2017.

[19] K. Hockel and M. U. Schuhmann, "ICP monitoring by open extra-ventricular drainage: Common practice but not suitable for advanced neuromonitoring and prone to false negativity," *Acta Neurochir. Suppl.*, vol. 126, pp. 281–286, 2018.

[20] H. A. Wilkinson *et al.*, "Erroneous measurement of intracranial pressure caused by simultaneous ventricular drainage: a hydrodynamic model study," *Neurosurg.*, vol. 24, no. 3, pp. 348–354, 1989.

[21] A. A. Birch *et al.*, "Erroneous intracranial pressure measurements from simultaneous pressure monitoring and ventricular drainage catheters," *Neurocrit. Care*, vol. 5, no. 1, pp. 51–54, 2006.

[22] S. Lee *et al.*, "Enhanced wall shear stress prevents obstruction by astrocytes in ventricular catheters," *J. Royal Soc. Interface*, vol. 17, no. 168, p. 20190884, 2020.

[23] I. T. Gabe, "Pressure measurement in experimental physiology," in *Cardiovascular Fluid Dynamics*. Elsevier, 1972, pp. 11–50.

[24] K. E. Latimer and R. D. Latimer, "Measurements of pressure-wave transmission in liquid-filled tubes used for intravascular blood-pressure recording," *Med. Biol. Eng.*, vol. 7, no. 2, pp. 143–168, 1969.

[25] J. K. Li *et al.*, "Fluid-filled blood pressure measurement systems," *J. Appl. Physiol.*, vol. 40, no. 5, pp. 839–843, 1976.

[26] D. L. Fry *et al.*, "An evaluation of modern pressure recording systems," *Circ. Res.*, vol. 5, no. 1, pp. 40–46, 1957.

[27] L. J. Krovetz *et al.*, "Limitation of correction of frequency dependent artefact in pressure recordings using harmonic analysis," *Circ.*, vol. 50, no. 5, pp. 992–997, 1974.

[28] R. M. Gardner, "Direct blood pressure measurement–dynamic response requirements," *Anesthesiol.*, vol. 54, no. 3, pp. 227–236, 1981.

[29] L. A. Geddes and J. D. Bourland, "Estimation of the damping coefficient of fluid-filled, catheter-transducer pressure-measuring systems," *J. Clin. Eng.*, vol. 13, no. 1, pp. 59–66, 1988.

[30] B. Kleinman, "Understanding natural frequency and damping and how they relate to the measurement of blood pressure," *J. Clin. Monit.*, vol. 5, no. 2, pp. 137–147, 1989.

[31] L. T. Hersh *et al.*, "Evaluation of filtering methods for acquiring radial intra-artery blood pressure waveforms," *J. Clin. Monit. Comput.*, vol. 29, no. 5, pp. 659–669, 2015.

[32] H. van Langen *et al.*, "Dynamic response of a neonatal catheter-manometer system in situ," *J. Clin. Monit.*, vol. 9, no. 5, pp. 335–340, 1993.

[33] D. M. Chernoff, "Frequency analysis of catheter systems used for invasive blood pressure monitoring," B.S. and M.S. thesis, Dept. Elect. Eng. and Comp. Sc., MIT, Cambridge, MA, 1982.

[34] W. L. Henry *et al.*, "A calibrator for detecting bubbles in cardiac catheter-manometer systems," *J. Appl. Physiol.*, vol. 23, no. 6, pp. 1007–1009, 1967.

[35] H. Takizawa *et al.*, "Spectral analysis of the CSF pulse wave at different locations in the craniospinal axis," *J. Neurol. Neurosurg. Psych.*, vol. 49, no. 10, pp. 1135–1141, 1986.

[36] J. V. Hickey *et al.*, "Intracranial pressure waveform analysis during rest and suctioning," *Biol. Res. Nurs.*, vol. 11, no. 2, pp. 174–186, 2009.

[37] M. Chopp and H. D. Portnoy, "Systems analysis of intracranial pressure. comparison with volume-pressure test and CSF-pulse amplitude analysis," *J. Neurosurg.*, vol. 53, no. 4, pp. 516–527, 1980.

[38] H. D. Portnoy and M. Chopp, "Cerebrospinal fluid pulse wave form analysis during hypercapnia and hypoxia," *Neurosurg.*, vol. 9, no. 1, pp. 14–27, 1981.

[39] A. C. Lapointe and F. A. Roberge, "Mechanical damping of the manometric system used in the pressure gradient technique," *IEEE Trans. Biomed. Eng.*, vol. 21, no. 1, pp. 76–78, 1974.

[40] I. R. Piper *et al.*, "Automated time-averaged analysis of craniospinal compliance (short pulse response)," *Acta Neurochir. Suppl.*, vol. 51, pp. 387–390, 1990.

[41] E. S. Lin *et al.*, "Systems analysis applied to intracranial pressure waveforms and correlation with clinical status in head injured patients," *Brit. J. Anaesth.*, vol. 66, no. 4, pp. 476–482, 1991.

[42] E. L. Foltz and C. Aine, "Diagnosis of hydrocephalus by csf pulse-wave analysis: a clinical study," *Surg. Neurol.*, vol. 15, no. 4, pp. 283–293, 1981.

[43] C. Anile *et al.*, "A new method of estimating intracranial elastance," *Interdisc. Neurosurg.*, vol. 1, no. 2, pp. 26–30, 2014.

[44] T. J. Cross *et al.*, "Correcting the dynamic response of a commercial esophageal balloon-catheter," *J. Appl. Physiol.*, vol. 121, no. 2, pp. 503–511, 2016.

This work is licensed under a Creative Commons Attribution-NonCommercial-NoDerivatives 4.0 License. For more information, see https://creativecommons.org/licenses/by-nc-nd/4.0/